ASTM INTERNATIONAL

Journal of
Testing and Evaluation

A. N. Amirkhanian,[1] D. W. Spring,[2] J. R. Roesler,[2] and G. H. Paulino[3]

DOI: 10.1520/JTE20140312

Forward and Inverse Analysis of Concrete Fracture Using the Disk-Shaped Compact Tension Test

VOL. 44 / NO. 1 / JANUARY 2016

Journal of Testing and Evaluation

doi:10.1520/JTE20140312 / Vol. 44 / No. 1 / January 2016 / available online at www.astm.org

A. N. Amirkhanian,[1] D. W. Spring,[2] J. R. Roesler,[2] and G. H. Paulino[3]

Forward and Inverse Analysis of Concrete Fracture Using the Disk-Shaped Compact Tension Test

Reference

Amirkhanian, A. N., Spring, D. W., Roesler, J. R., and Paulino, G. H., "Forward and Inverse Analysis of Concrete Fracture Using the Disk-Shaped Compact Tension Test," *Journal of Testing and Evaluation*, Vol. 44, No. 1, 2016, pp. 625–634, doi:10.1520/JTE20140312. ISSN 0090-3973

ABSTRACT

A new concrete fracture geometry is presented, which can quantify multiple fracture properties from a single specimen test. The disk-shaped compact tension (DCT) geometry allows specimens to be fabricated from laboratory cylinders or field cores. The DCT fracture test characterizes the concrete's critical stress intensity factor, K_{IC}, critical crack-tip opening displacement, $CTOD_c$, and initial fracture energy, G_f, as well as the specimen-dependent total fracture energy, G_F. The DCT-based fracture properties have the same experimental variation as the single-edge notched beam test. The experimentally derived fracture parameters were implemented into a cohesive zone model, which enabled estimation of concrete tensile strength from field-extracted cores.

Keywords

concrete fracture, inverse analysis, concrete characterization

Manuscript received August 11, 2014; accepted for publication May 5, 2015; published online September 3, 2015.

[1] Dept. of Civil and Environmental Engineering, Univ. of Illinois at Urbana–Champaign, 205 North Mathews Ave., Urbana, IL 61801, United States of America (Corresponding author), e-mail: amirkha1@illinois.edu

[2] Dept. of Civil and Environmental Engineering, Univ. of Illinois at Urbana–Champaign, 205 North Mathews Ave., Urbana, IL 61801, United States of America.

[3] Dept. of Civil and Environmental Engineering, Georgia Institute of Technology, 790 Atlantic Dr. NW, Atlanta, GA 30332, United States of America. (Formerly at Univ. of Illinois at Urbana-Champaign, Urbana, IL 61801, United States of America.)

Introduction

Current design practices for concrete structures are usually based on strength criteria, e.g., compressive, flexural, or tensile strength, without consideration of size and geometric effects. Fracture mechanics provides a method to characterize a concrete material so that the properties are independent of size and geometry. These fracture properties can be used in advanced numerical models to accurately predict the behavior of a concrete structure. Current impediments to using fracture mechanics in civil engineering are the selection of the test specimen geometry, the available equipment to run the test, and the analysis and design tools to widely apply the fracture properties.

One of the first specimen geometries used for concrete fracture testing was the three-point or single-edge notched beam (SEN(B)) [1]. Beams are readily cast in a laboratory setting and preparation only involves cutting a notch, which has led to extensive testing with SEN(B) specimens. With the need to evaluate the in situ load capacity of a structure, field-extracted samples are desired. Although SEN(B) specimens are manageable in the lab, attempting to extract beams from the field is difficult and costly. Alternatively, cores can be easily extracted from a concrete structure. Motivated by previous work on asphalt concrete specimens [2], a geometry was chosen that is simple to fabricate and produces consistent and accurate results. The disk-shaped compact tension (DCT) geometry has been used extensively in the metals and ceramic field [3,4], as well as with asphalt concrete [5–7] materials with consistent and accurate results, allowing for a direct comparison between different mixtures. The DCT geometry for asphaltic materials is also adopted as a standard now in ASTM D7313-13 [32]. Past researchers have used a compact tension (CT) geometry for concrete [8–11] or a round double-beam geometry [12], but the use of the DCT specimen for concrete has not been explored. The main advantage of the DCT specimen geometry, and the primary motivation for this work, is that it can be easily fabricated from a laboratory cylinder or field core.

Research Objective

The objective of this research is to develop a test procedure for determining the fracture and strength properties of concrete using the DCT specimen. Geometric correction factors for the DCT test configuration are required to extract the fracture parameters from the experimental data. The calculated fracture parameters can then be input to a cohesive zone model (CZM) to predict the entire fracture behavior of DCT specimens with different concrete mixtures. Inverse analysis with a validated CZM can be used to estimate the in situ tensile strength of a concrete structure.

Experimental Procedures

A preliminary DCT specimen geometry taken from Tada et al. [13] was adopted because it had existing geometric correction factors published that could easily implemented for concrete [14]. However, it had a significantly shorter ligament length than the newly approved ASTM D7313-13 [32] geometry. To increase the size of the fracture area, the longer ligament length in the ASTM geometry was chosen for this study. The newly proposed DCT geometry is illustrated in **Fig. 1** and summarized in **Table 1**. This DCT geometry can be prepared from standard 6-in. (152-mm) diameter cores or cast using 6 in. (152 mm) by 12 in. (304 mm) cylinder molds.

FIG. 1 DCT geometry (a) and test setup configuration (b).

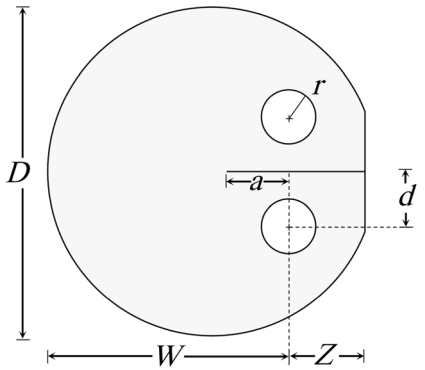

(a)

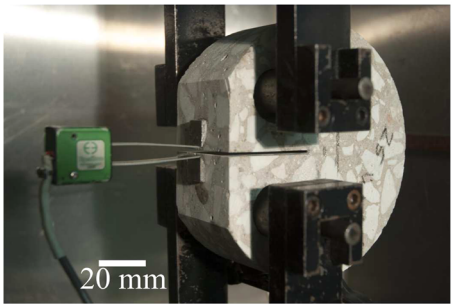

(b)

DCT specimens are tested at room temperature using a closed-loop servo-hydraulic testing frame. A seating load of 0.2 kN is applied and the test is controlled using a crack mouth opening displacement (CMOD) rate of 0.001 mm/s. After the peak load is reached, the specimen is unloaded at a rate of 0.5 kN/s to the seating load of 0.2 kN to capture the unloading compliance. The specimen is then immediately reloaded monotonically at the original CMOD rate of 0.001 mm/s until the specimen reaches a final capacity equal to the seating load. Though the geometry is different, the loading and unloading compliances are measured in the same manner as in the SEN(B) procedure [15]. The loading compliance is the inverse of the slope of the initial loading portion of the test (up to 50 %

TABLE 1 DCT geometry dimensions.

Dimension	Value, mm	Value, in.
D	152.0	6.0
W	110.0	4.3
Z	35.0	1.4
d	25.0	1.0
a	27.5	1.1
r	12.5	0.5
B (specimen thickness)	51.0	2.0
n (saw-blade thickness)	1.3	0.05
h (knife-edge thickness)	3.0	0.1

FIG. 2 Typical loading and unloading compliances of DCT specimen.

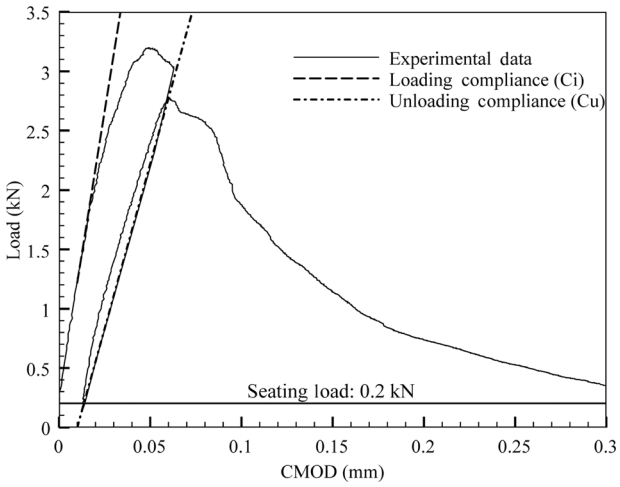

of the peak load). The unloading compliance is the inverse of the slope of the unloading portion from 80 % to 20 % of the peak load. An example data set is provided in **Fig. 2** to illustrate the loading and unloading procedure.

Different concrete mixes, as detailed in **Table 2**, were utilized for fabricating the DCT specimens from cored or cast cylinders. Mixture S-1 is a concrete paving mixture used in an outdoor pavement test section. The S-2 mixtures were used for a slab load testing comparison between concrete containing virgin aggregates (S-2a) and recycled concrete aggregate (RCA) (S-2b). The S-3 concrete mixtures were comparing a virgin aggregate (S-3a) with a fractionated reclaimed asphalt pavement (FRAP) mixture (S-3b). Finally, mixture S-4 is a concrete mixture containing virgin aggregates and ground granulated blast furnace slag (GGBFS).

As noted in **Tables 2** and **3**, the mixtures and test specimens were obtained from different projects and thus were subjected to varying curing and environmental conditions. The specimens were selected to validate the DCT test method over a range of concrete mixture proportions and curing conditions.

TABLE 3 Environmental and curing conditions along with specimen preparation technique for the various DCT test sets.

Factor	S-1	S-2	S-3	S-4
Testing ages, days	710, 1578	223, 591	142	40
Curing condition	Outdoors	Outdoors, lime bath	Moist room	Lime bath
Specimen preparation	Cored	Cored, cast	Cast	Cast

Furthermore, several of the specimens were prepared from field-extracted cores, whereas others came from cast cylinders (see **Table 3**). The initial specimen age at testing was selected to avoid time-dependent concrete fracture properties. A longer testing age was selected for a few mixtures to determine the fracture and strength properties of a more mature concrete pavement.

Calculation of Fracture Properties

The first step in determining the concrete fracture properties from the DCT specimen is to find the critical crack length ratio based on the specimen's peak load, compliance measurements, and geometric factors. The crack length ratio, α, is given by Eq 1, which corrects for the gauge point thickness (h).

$$\alpha = \frac{a + h}{W + h} \tag{1}$$

Because the critical crack length ratio (α_c) at the peak load is not known, the measured loading and unloading compliances are used to determine this unknown parameter. The elastic modulus (E) of the bulk concrete is assumed to remain constant after the initial crack length (a_o) propagates. The elastic modulus can be calculated by Eq 2, where $C_{i,u}$ is the compliance, either loading or unloading, of the specimen and $V_{CMOD}(\alpha)$ is the DCT crack opening geometric correction factor defined by Eq 3. The correction factor was determined from

TABLE 2 Mixture designs for all DCT specimens tested, lb/yd^3 (kg/m^3).

Constituent	S-1	S-2a	S-2b	S-3a	S-3b	S-4
Cement	421 (250)	484 (287)	484 (287)	380 (225)	380 (225)	335 (199)
Fly ash	140 (83)	116 (69)	116 (69)	90 (53)	90 (53)	61 (36)
GGBFS	–	–	–	115 (68)	115 (68)	213 (126)
Limestone CA[a]	1903 (1129)	1402 (832)	–	1750 (1038)	1375 (816)	1307 (775)
RCA CA	–	–	1278 (758)	–	–	–
FRAP CA	–	–	–	–	375 (222)	–
Limestone IA[b]	–	469 (278)	462 (274)	–	–	560 (332)
Natural sand	1214 (720)	1247 (740)	1234 (732)	1326 (787)	1326 (787)	1216 (721)
Water	236 (140)	238 (141)	238 (141)	245 (145)	245 (145)	226 (134)

[a]CA = Coarse aggregate.
[b]IA = Intermediate aggregate.

a numerical analysis because there were no published factors available for this particular geometry. Once the loading and unloading compliances, as well as the initial crack length ratio, α_o, are determined, the critical crack length ratio, α_c, is calculated by assuming equivalent elastic moduli in the loading and unloading cycles (Eq 4).

$$E = \frac{2V_{\mathrm{CMOD}}(\alpha)}{C_{i,u}B} \tag{2}$$

$$V_{\mathrm{CMOD}}(\alpha) = \frac{501.8\alpha^3 + 2294\alpha^2 + 4349\alpha + 1384}{\alpha^4 + 272.2\alpha^3 - 139.8\alpha^2 - 569.3\alpha + 433.9} \tag{3}$$

$$V_{\mathrm{CMOD}}(\alpha_c) = \frac{C_u}{C_i} V_{\mathrm{CMOD}}(\alpha_o) \tag{4}$$

With the critical crack length ratio known, the critical stress intensity factor (K_{IC}) is calculated using Eq 5, where:

σ = the nominal stress at the peak load,

P = the peak load, and

$F(\alpha_c)$ = the K_{IC} geometric correction factor (Eq 7) derived from the numerical analysis.

The critical stress intensity factor, K_{IC}, describes a material's resistance to fracture. When linear elastic fracture mechanics (LEFM) are valid, the critical stress intensity factor is a material property and is independent of the specimen geometry:

$$K_{\mathrm{IC}} = \sigma\sqrt{W}F(\alpha_c) \tag{5}$$

$$\sigma = \frac{P}{WB} \tag{6}$$

$$F(\alpha_c) = \frac{-1.498\alpha^3 + 4.569\alpha^2 - 1.078\alpha + 0.113}{\alpha^4 - 2.408\alpha^3 + 1.717\alpha^2 - 0.3467\alpha + 0.0348} \tag{7}$$

For most concrete specimen sizes including this DCT geometry, LEFM does not produce size-independent fracture properties and, thus, nonlinear elastic fracture mechanics (NLFM) was developed to extract multiple size independent fracture parameters [16,17]. The second fracture parameter, the critical crack tip opening displacement (CTOD_c), is calculated using Eq 8, where $V_{\mathrm{CTOD}}(\alpha)$ is given by Eq 9 and determined through numerical analysis. The CTOD_c, combined with the critical stress intensity factor, K_{IC}, constitute the NLFM model known as the two-parameter fracture model [17]:

$$\mathrm{CTOD}_c = \frac{2\sigma W V_{\mathrm{CTOD}}(\alpha_c)}{E} \tag{8}$$

$$V_{\mathrm{CTOD}}(\alpha) = \frac{6.639\alpha^3 - 3.209\alpha^2 + 0.4169\alpha - 0.006899}{\alpha^4 - 2.429\alpha^3 + 1.897\alpha^2 - 0.5137\alpha + 0.04504} \tag{9}$$

All three geometric correction factors (Eqs 3, 7, and 9) that were determined numerically for the ASTM D7313-13 [32] specimen are valid for an a/W ratio ranging from 0.22 to 0.84. Two other useful fracture parameters, the initial fracture energy, G_f, and total fracture energy, G_F, can be determined from the experimental data. The total fracture energy of the concrete measures the total amount of energy required to separate two crack surfaces [18,19] despite its known specimen-size dependency. The total fracture energy is calculated from the area under the load-CMOD curve normalized to the uncracked ligament area [20], whereas the initial fracture energy is defined by Eq 10 for plane stress.

$$G_f = \frac{K_{\mathrm{IC}}^2}{E} \tag{10}$$

Numerical Modeling

To predict the fracture behavior of concrete with the DCT specimen geometry given any set of fracture properties, a nonlinear finite-element model is created to simulate the crack growth. Previous work suggests that a cohesive zone model with a bilinear softening relation can adequately describe the fracture behavior of plain concrete [21–28]. **Fig. 3** illustrates the finite-element mesh used to simulate the mode I fracture of the DCT specimen. The bulk material is modeled with linear elastic elements (Q4), whereas the fracture behavior is captured using 2D cohesive elements. The cohesive elements are inserted in front of the initial notch tip, along the expected mode I fracture path of the specimen, and have zero thickness in the un-deformed configuration. To model the nonlinear fracture process accurately, the size of the cohesive zone elements was determined to be 0.7 mm.

The cohesive zone model is implemented in commercial software (e.g., ABAQUS) as a user-defined subroutine. The bilinear softening model, shown in **Fig. 3**, is used to idealize the traction–separation relationship in front of the macro-crack tip. The inputs to the bilinear softening model are the tensile strength, f_t; the initial and total fracture energies, G_f and G_F respectively; the ratio of the kink point, ψ; and a parameter defining penalty stiffness, p. The kink point [28] is located at $(w_k, \psi f_t')$ where:

$$w_k = \mathrm{CTOD}_c \tag{11}$$

$$\psi = 1 - \frac{\mathrm{CTOD}_c f_t'}{2G_f} \tag{12}$$

There have been many proposed locations for the stress ratio at the kink point (ψ), most of which vary between 0.15 and 0.33, with little agreement on the precise location. Park et al. [28] showed that, by assuming the crack opening width at the kink point to be that in Eq 11, the stress ratio could be consistently calculated based on experimentally determined parameters. The penalty stiffness, p, defines the ratio of the opening displacement at the peak load, w_{cr}, to the final opening displacement, w_f. The value of the penalty stiffness is based on numerical stability considerations and a parametric analysis demonstrated converged

FIG. 3 DCT specimen with bulk and cohesive zone finite-element mesh (a) and cohesive stress-opening relation with bilinear softening (b) (Ref 25). Because the cohesive elements initially have zero thickness, they are only implicitly represented, along the horizontal line ahead of the notch tip.

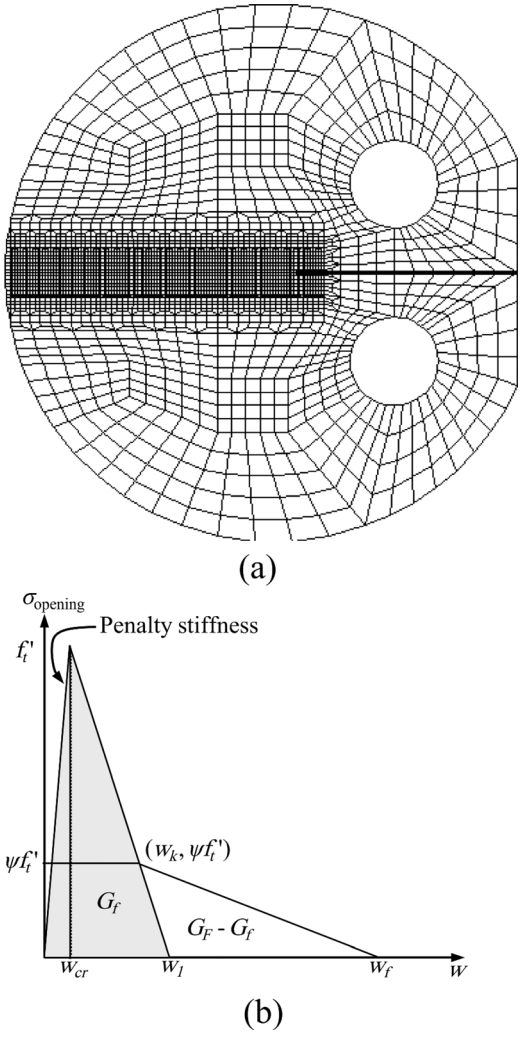

results when $p \leq 0.01$. With the measured fracture properties and tensile strength data, the load-CMOD behavior for the different concrete mixtures can be predicted and compared with the experiments.

TABLE 5 Input parameters for the numerical model.

Mix	Age, Days	E, GPa	G_f, N/m	G_F, N/m	f_t, MPa	ψ	p
S-2a	591	50.0	72.3	140.8	6.6	0.030	0.01
S-3a	142	36.0[a]	49.1	120.3	4.8	0.179	0.01
S-3b	142	30.8[a]	42.2	119.0	3.8	0.209	0.01
S-4	40	29.0[a]	32.4	111.7	4.0	0.113	0.01

Note: The elastic modulus (E) values were measured following ASTM C469-14 [30] and the tensile strength values, f_t, were measured following ASTM C496-11 [31]. The strength values were measured at the same age as the fracture properties.
[a]Estimated modulus using Eq 2.

Results and Discussion

The experimental fracture results for the various mixtures and test ages are summarized in **Table 4**. The calculated fracture parameters for the DCT specimen fall within the typical range of normal strength concrete. The second fracture parameter, $CTOD_c$, has the highest coefficient of variation (COV). Additionally, the initial fracture energy, G_f, has a high COV because it is based on the calculated value of K_{IC} and E. This is not unusual, as it has been shown in the literature that these fracture parameters, determined from various fracture tests, have COV values in this range [29].

The numerical analysis of the DCT test specimens is separated into two parts. In the first part, the experimental load-CMOD results are compared with the numerical results using the measured indirect tensile strength and fracture properties. In the second part, an inverse analysis is performed to derive the tensile strength of the concrete given the experimental fracture parameters and validated numerical model. The modeling assumptions used in the numerical analysis are listed in **Table 5**. In several mixtures, the elastic modulus was not directly measured but calculated from the DCT loading compliance using Eq 2.

NUMERICAL MODELING: FORWARD ANALYSIS

The DCT load-CMOD results from the experimental and numerical investigations are compared in **Figs. 4–6** for the five mixture sets listed in **Table 5**. The results from the numerical

TABLE 4 Experimental DCT fracture results for all specimens with mean values (coefficient of variation) and number of specimens.

Mix	Age, Days	Total Spec.	K_{IC}, MPa · m$^{1/2}$	$CTOD_c$, mm	G_f, N/m	G_F, N/m
S-1	710	18	1.02 (14 %)	0.0122 (29 %)	29.9 (30 %)	125.2 (19 %)
S-1	1578	6	1.66 (10 %)	0.0254 (18 %)	72.3 (17 %)	148.0 (14 %)
S-2a	223	4	1.02 (14 %)	0.0172 (35 %)	31.8 (31 %)	114.4 (16 %)
S-2b	223	4	1.02 (14 %)	0.0256 (35 %)	43.3 (28 %)	162.7 (11 %)
S-2a	591	4	1.67 (13 %)	0.0212 (31 %)	72.3 (26 %)	140.8 (15 %)
S-3a	142	8	1.33 (8 %)	0.0167 (8 %)	49.1 (15 %)	120.3 (30 %)
S-3b	142	8	1.14 (10 %)	0.0176 (15 %)	42.2 (18 %)	119.0 (17 %)
S-4	40	3	0.97 (4 %)	0.0145 (6 %)	32.4 (12 %)	111.7 (14 %)

FIG. 4 Experimental and numerical results from S-2a concrete mixture at 591 days with virgin aggregates.

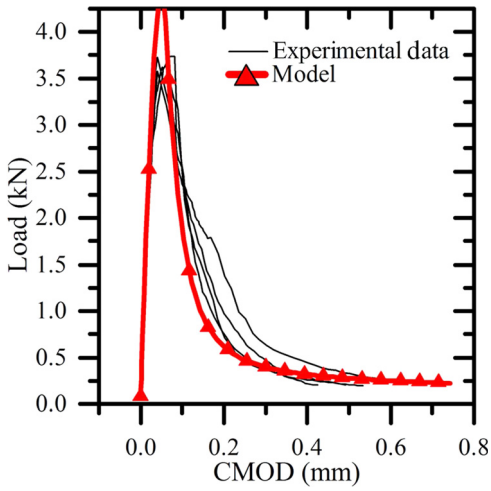

FIG. 5 Experimental and numerical results from S-3 concrete mixtures at 142 days with (a) virgin aggregates, and (b) recycled asphalt pavement aggregates.

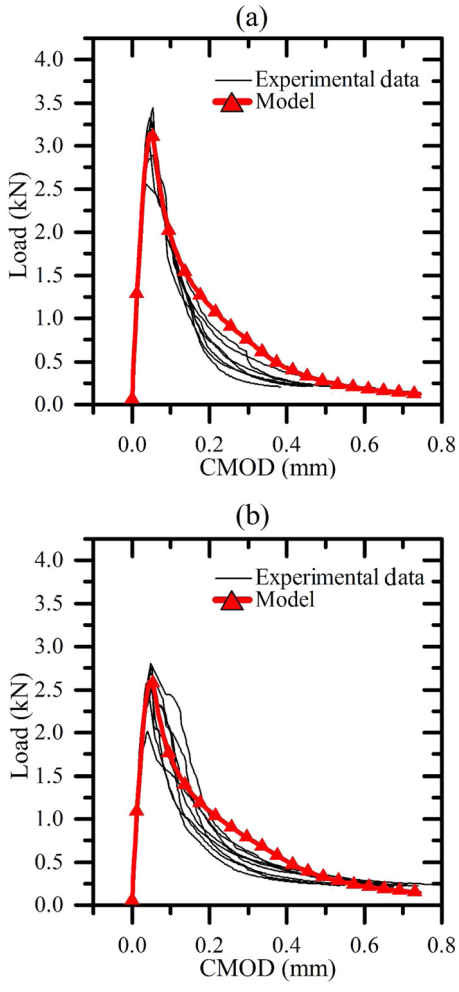

FIG. 6 Experimental and numerical results from S-4 concrete mixture at 40 days with GGBFS.

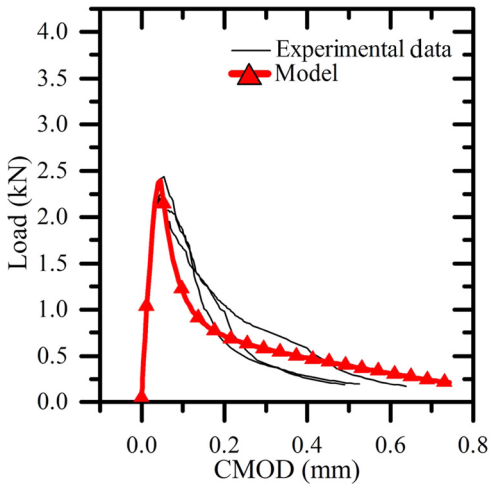

model are in reasonable agreement with the experimental results (**Table 6**).

Mixes S-1 (710 and 1578 days) and S-2 (223 days) had tensile strengths measured at different ages than the fracture properties listed in **Table 7**. In the case of mixture S-1, the tensile strength values are from 28 days versus the 710 - and 1578-day DCT test age. The S-2 (223 days) tensile strength values come from 220-day moist cured samples, whereas the fracture specimens were cored from slabs that were exposed to ambient weather conditions that including freezing and thawing cycles.

NUMERICAL MODELING: INVERSE ANALYSIS

The initial numerical analysis of the mixes proceeded with the assumption that all of the tensile strengths were correct for the DCT specimens (see **Figs. 7** and **8** and **Table 8**). There was especially significant mismatch between the experimental data and numerical model for mixture S-2. Because the results from **Table 6** validated the numerical model and test method, the experimental fracture data from the S-1 and S-2 mixtures at 223 days was used to perform an inverse analysis to determine the

TABLE 6 DCT peak load comparison between average experimental and numerical results.

Mix	Age, Days	Experimental, kN	Model, kN	Percent Diff.
S-1	710	2.48	2.77	11.7 %
S-1	1578	3.25	3.58	10.2 %
S-2a	223	2.09	3.42	63.6 %
S-2b	223	1.95	3.05	56.4 %
S-2a	591	3.69	4.41	16.3 %
S-3a	142	3.10	3.14	1.3 %
S-3b	142	2.58	2.59	0.4 %
S-4	40	2.31	2.39	3.3 %

TABLE 7 Initial and final strength parameters used in the inverse analysis to determine the tensile strength of the concrete mixtures.

Mix	Age, Days	E, GPa	G_f, N/m	G_F, N/m	f_t, MPa	ψ
S-1	710	40.6[a]	29.9	125.2	4.7[a]	0.041
					4.0[b]	0.184[b]
S-1	1578	40.6[a]	72.3	148.0	4.7[a]	0.174
					4.2[b]	0.262[b]
S-2a	223	50.0	31.8	114.4	4.9	0.250
					2.2[b]	0.405[b]
S-2b	223	40.1	43.3	162.7	4.6	0.250
					2.0[b]	0.408[b]

Note: Unless otherwise noted, the strength values were measured at the same age as the fracture properties.
[a]Values based on 28-day measured strengths.
[b]Determined from an inverse analysis based on the fracture properties.

FIG. 7 Experimental and numerical results from S-1 concrete mixture at (a) 710 days, and (b) 1578 days.

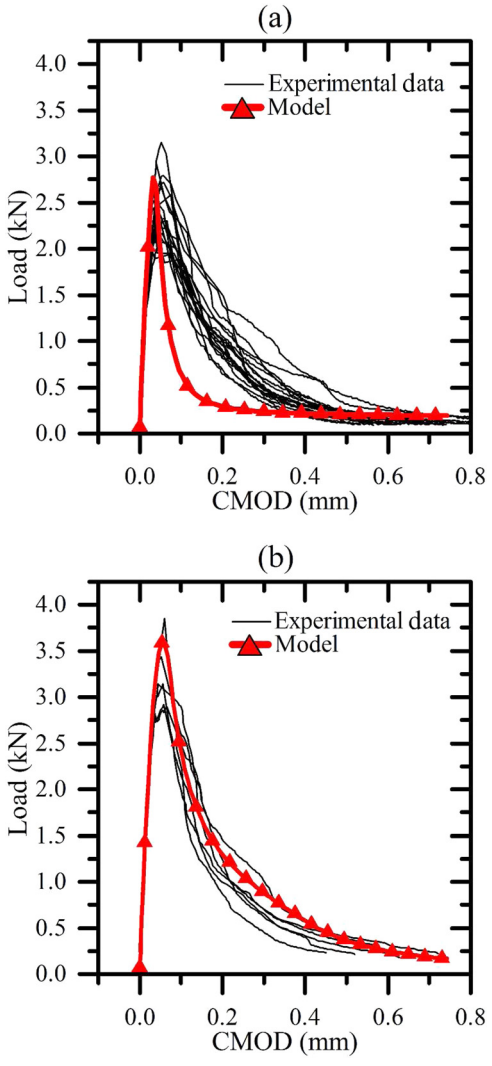

FIG. 8 Experimental and numerical results from S-2 concrete mixtures at 223 days with (a) virgin aggregates, and (b) recycled concrete aggregates.

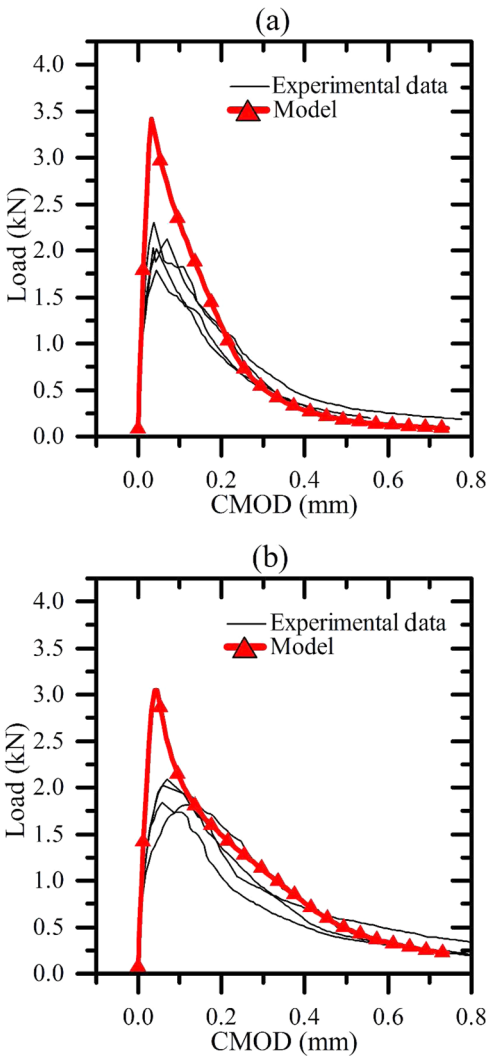

concrete's tensile strength. Based on the experimental load-CMOD curves of the DCT specimens, the tensile strength in the CZM was optimized to minimize the error between the experimental and numerical predictions of the peak load (see **Figs. 9** and **10** and **Table 8**).

As illustrated in **Figs. 9** and **10**, and listed in **Table 8**, the inverse analysis of the DCT specimen with the CZM successfully captures the peak load of the S-1 and S-2 mixtures if the fracture and strength properties of the concrete are known. The analysis shows that the S-1 mixtures had a lower tensile strength from the 28-day value. This was not unexpected because the fracture specimens came from cores of a test pavement section that was exposed to the outdoor environment up until coring. The tensile strength data measured at 28 days was from specimens that were moist cured, whereas the pavement section only had a curing compound applied to it. It has long been known

TABLE 8 Comparison of the experimentally and numerically determined peak loads when optimizing the cohesive strength to minimizing the error in the predicted versus actual peak load at specimen failure.

Mix	Age, Days	Experimental, kN	Initial Model, kN	Final Model, kN	Percent Difference (Initial)	Percent Difference (Final)
S-1	710	2.48	2.77	2.59	10.5 %	4.2 %
S-1	1578	3.25	3.58	3.37	9.2 %	3.6 %
S-2a	223	2.09	3.42	2.05	38.9 %	2.0 %
S-2b	223	1.95	3.05	1.95	36.1 %	0.0 %

that standard 28-day moist cured specimens do not accurately represent the in situ strength of a structure, especially if it was cured in a different manner.

This discrepancy is more prevalent in the S-2 mixtures at 223 days. The tensile strength specimens for these mixtures were moist cured for 220 days. The specimens that were cored for fracture testing were continuously exposed to the outdoor environment until testing and only had a curing compound applied to the surface. Although most agencies would not moist cure strength specimens for 220 days, this long curing duration shows that measured strength values are heavily influenced by curing conditions. This further illustrates the need for an accurate inverse analysis to determine the tensile strength. Until now, the only way to confirm the in situ tensile strength was to take a core. Measuring the tensile strength of a core can lead to high variability and skewed answers based on how smooth the

FIG. 9 Inverse analysis results of S-1 concrete mixture at (a) 710 days, and (b) 1578 days with calculated tensile strengths of 4.0 and 4.2 MPa, respectively.

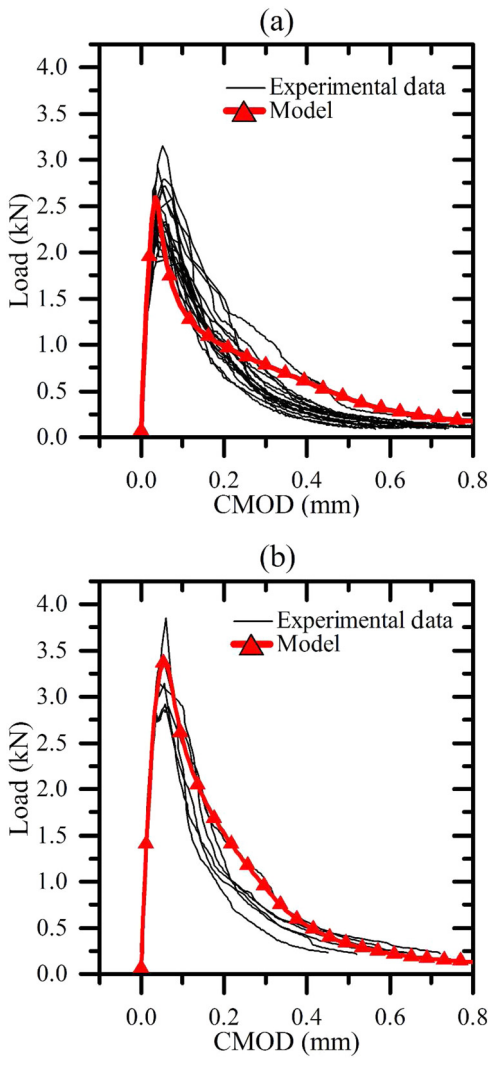

FIG. 10 Inverse analysis results of (a) S-2a, and (b) S-2b concrete mixtures at 223 days with calculated tensile strengths of 2.2 MPa and 2.0 MPa, respectively.

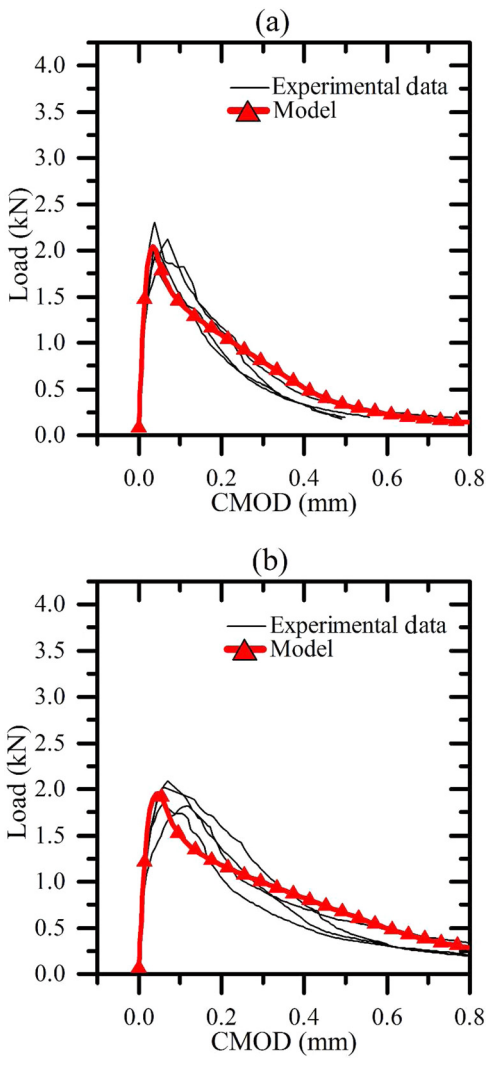

coring surface is. Measuring the fracture properties of the outdoor specimens provides an accurate assessment of the in situ tensile strength.

Upon first observation, it appears that the tensile strength of the S-2a mixture jumped from an in situ value of 2.2 MPa at 223 days to 6.6 MPa at 591 days. However, the fracture specimens tested at 591 days were cast cylinders that underwent the same curing regime as the tensile strength specimens. Because of this fact, the measured tensile strength at 591 days for the S-2a mixture is the true tensile strength of the fracture specimens, whereas the 2.2 MPa comes from the inverse analysis of the concrete specimens that had no moist curing and were exposed to the outdoor environment.

Conclusions

A new test method was used to characterize concrete fracture properties using the disk-shaped compact tension (DCT) geometry. The benefit of the DCT geometry is the ability to make fracture specimens from standard laboratory cylinders or field-extracted cores. A variety of concrete mixtures were tested at different ages and curing conditions. The experimental fracture parameters and variation was similar to previously reported tests of normal strength concrete.

Numerical simulations using a cohesive crack element were successful in predicting the load-CMOD response curves if the fracture properties and tensile strength of the concrete were known with reasonable accuracy. As expected, DCT specimens without an accurate measure of tensile strength could not reproduce the experimental load-CMOD curves. However, an inverse analysis of the DCT specimen with the measured fracture parameters was able to estimate the concrete tensile strength by minimizing the error between the actual and predicted peak loads. For many structures, obtaining the proper sized cores for tensile or compressive strength determination may be difficult. The DCT inverse analysis allows for the tensile strength of an existing structure to be estimated from the DCT fracture test.

ACKNOWLEDGMENTS

The writers acknowledge the support from the National Science Foundation (NSF) through Grant CMMI #0800805. The information presented in this paper is the sole opinion of the authors and does not necessarily reflect the views of the sponsoring agency.

References

[1] Keat, L. B., "Fracture of Concrete," Master's thesis, Massachusetts Institute of Technology, Cambridge, MA, 1967.

[2] Wagoner, M. P., Buttlar, W. G., and Paulino, G. H., "Disk-Shaped Compact Tension Test for Asphalt Specimens," *Exp. Mech.*, Vol. 45, No. 3, 2005, pp. 270–277.

[3] Gilbert, C. J., McNaney, J. M., Dauskardt, R. H., and Ritchie, R. O., "Back-Face Strain Compliance and Electrical-Potential Crack Length Calibrations for the Disk-Shaped Compact Tension DC(T) Specimen," *J. Test. Eval.*, Vol. 22, No. 2, 1994, pp. 117–120.

[4] Chen, D., Gilbert, C. J., and Ritchie, R. O., "In Situ Measurement of Fatigue Crack Growth Rates in a Silicon Carbide Ceramic at Elevated Temperatures Using a DC Potential System," *J. Test. Eval.*, Vol. 28, No. 4, 2000, pp. 236–241.

[5] Wagoner, M. P., Buttlar, W. G., Paulino, G. H., and Blankenship, P. I., "Laboratory Testing Suite for Characterization of Asphalt Concrete Mixtures Obtained from Field Cores," *J. Assoc. Asphalt Paving Technol.*, Vol. 75, 2006, pp. 815–852.

[6] Zofka, A. and Braham, A., "Comparison of Low-Temperature Field Performance and Laboratory Testing of 10 Test Sections in the Midwestern United States," *Transport. Res. Rec.*, No. 2127, 2009, pp. 107–114.

[7] Kim, M., Buttlar, W. G., Baek, J., and Al-Qadi, I. L., "Field and Laboratory Evaluation of Fracture Resistance of Illinois Hot-Mix Asphalt Overlay Mixtures," *Transport. Res. Rec.*, No. 2127, 2009, pp. 146–154.

[8] Van Mier, J. G. M., "Mode I Fracture of Concrete: Discontinuous Crack Growth and Crack Interface Grain Bridging," *Cement Concrete Res.*, Vol. 21, No. 1, 1991, pp. 1–15.

[9] Issa, M. A., Islam, M. S., and Chudnovsky, A., "Size Effects in Concrete Fracture. Part I: Experimental Setup and Observations," *Int. J. Fract.*, Vol. 102, No. 1, 2000, pp. 1–24.

[10] Issa, M. A., Islam, M. S., and Chudnovsky, A., "Size Effect in Concrete Fracture. Part II: Analysis of Test Results," *Int. J. Fract.*, Vol. 102, No. 1, 2000, pp. 15–42.

[11] Kumar, S. and Barai, S. V., "Determining Double-K Fracture Parameters of Concrete for Compact Tension and Wedge Splitting Tests Using Weight Function," *Eng. Fract. Mech.*, Vol. 76, No. 7, 2009, pp. 935–948.

[12] Hanson, J. H. and Ingraffea, A. R., "Compression Loading Applied to Round Double-Beam Fracture Specimens. I: Application to Materials With Large Characteristic Lengths," *J. Test. Eval.*, Vol. 30, No. 6, 2002, pp. 508–514.

[13] Tada, H., Paris, P. C., and Irwin, G. R., *The Stress Analysis of Cracks Handbook*, ASME, New York, 2000.

[14] Amirkhanian, A., Spring, D., Roesler, J., and Paulino, G., "Disk-Shaped Compact Tension Test for Plain Concrete," *ASCE T&DI Congress*, Chicago, IL, March 13–16, 2011, pp. 688–698.

[15] RILEM, "Determination of Fracture Parameters (K_{IC} and $CTOD_C$) of Plain Concrete Using Three-Point Bend Tests," RILEM Committee on Fracture Mechanics of Concrete-Test Methods, *Mater. Struct.*, Vol. 23, No. 138, 1990, pp. 457–460.

[16] Bažant, Z. P. and Oh, B. H., "Crack Band Theory for Fracture of Concrete," *Mater. Struct./Materiaux et Constructions*, Vol. 16, No. 3, 1983, pp. 155–177.

[17] Jenq, Y. S. and Shah, S. P., "Two-Parameter Fracture Model for Concrete," *J. Eng. Mech.*, Vol. 111, No. 10, 1985, pp. 1227–1241.

[18] Hillerborg, A., Moder, M., and Petersson, P.-E., "Analysis of Crack Formation and Crack Growth in Concrete by Means of Fracture Mechanics and Finite Elements," *Cement Concrete Res.*, Vol. 6, No. 6, 1976, pp. 773–781.

[19] Peterson, P. E., "Fracture Energy of Concrete: Method of Determination," *Cement Concrete Res.*, Vol. 10, No. 1, 1980, pp. 79–89.
[20] Hillerborg, A., "The Theoretical Basis of a Method to Determine the Fracture Energy (GF) of Concrete," *Mater. Struct./Materiaux et Constructions*, Vol. 18, No. 4, 1985, pp. 291–296.
[21] Petersson, P. E., "Crack Growth and Development of Fracture Zone in Plain Concrete and Similar Materials," *Report No. TVBM-1006*, Division of Building Materials, Lund Institute of Technology, Lund, Sweden, 1981.
[22] Gustafsson, A. and Hillerborg, P. J., "Improvements in Concrete Design Achieved Through Application of Fracture Mechanics," *Appl. Fract. Mech. Cement. Compos.*, Vol. 94, 1985, pp. 639–680.
[23] Wittmann, F. H., Rokugo, K., Brühwiler, E., Mihashi, H., and Simopnin, P., "Fracture Energy and Strain Softening of Concrete as Determined by Compact Tension Specimens," *Mater. Struct.*, Vol. 21, No. 1, 1988, pp. 21–32.
[24] Guinea, G. V., Planas, J., and Elices, M., "A General Bilinear Fit for the Softening Curve of Concrete," *Mater. Struct.*, Vol. 27, No. 2, 1994, pp. 99–105.
[25] Bažant, Z. P., "Concrete Fracture Models: Testing and Practice," *Eng. Fract. Mech.*, Vol. 69, No. 2, 2002, pp. 165–205.
[26] de Borst, R., Gutierrez, M. A., Wells, G. N., Remmers, J. J. C., and Askes, H., "Cohesive Zone Models, Higher-Order Continuum Theories and Reliability Methods for Computational Failure Analysis," *Int. J. Numer. Methods Eng.*, Vol. 60, No. 1, 2004, pp. 289–315.
[27] Roesler, J. R., Paulino, G. H., Park, K., and Gaedicke, C., "Concrete Fracture Prediction Using Bilinear Softening," *Cement Concrete Compos.*, Vol. 29, No. 4, 2007, pp. 300–312.
[28] Park, K., Paulino, G. H., and Roesler, J. R., "Determination of the Kink Point in the Bilinear Softening Model for Concrete," *Eng. Fract. Mech.*, Vol. 75, No. 13, 2008, pp. 3806–3818.
[29] Bažant, Z. P., Qiang, Y., and Goanseup, Z., "Choice of Standard Fracture Test for Concrete and Its Statistical Evaluation," *Int. J. Fract.*, Vol. 118, No. 4, 2002, pp. 303–337.
[30] ASTM C469-14: Standard Test Method for Static Modulus of Elasticity and Poisson's Ratio of Concrete in Compression, ASTM International, West Conshohocken, PA, 2014, www.astm.org
[31] ASTM C496-11: Standard Test Method for Splitting Tensile Strength of Cylindrical Concrete Specimens, ASTM International, West Conshohocken, PA, 2014, www.astm.org
[32] ASTM D7313-13: Standard Method for Determining Fracture Energy of Asphalt-Aggregate Mixtures Using the Disk-Shaped Compact Tension Geometry, ASTM International, West Conshohocken, PA, 2013, www.astm.org